AFRL-VS-TR-2001-1660

Space Systems Environmental Interaction Studies

M. Alan Morgan
Alan C. Huber
David J. Sperry
Alan N. Donkin, Jr.
Scott J. Moran
Robert H. Redus
John A. Pantazis

AMPTEK, Inc.
6 DeAngelo Drive
Bedford, MA 01730

30 August 2000

Scientific Report No. 4

AIR FORCE RESEARCH LABORATORY
Space Vehicles Directorate
29 Randolph Rd
AIR FORCE MATERIEL COMMAND
Hanscom AFB, MA 01731-3010

" This technical report has been reviewed and is approved for publication."

WALLACE R. TURNBULL, Capt, USAF
Contract Manager

GREGORY P. GINET, Chief
Space Weather Center of Excellence

This report has been reviewed by the ESC Public Affairs Office (PA) and is releasable to the National Technical Information Service (NTIS).

Qualified requestors may obtain additional copies from the Defense Technical Information Center (DTIC). All others should apply to the National Technical Information Service (NTIS).

If your address has changed, if you wish to be removed from the mailing list, of if the addressee is no longer employed by your organization, please notify PL/IM, 29 Randolph Road, Hanscom AFB, MA. 01731-3010. This will assist us in maintaining a current mailing list.

Do not return copies of this report unless contractual obligations or notices on a specific document require that it be returned.

REPORT DOCUMENTATION PAGE

Form Approved
OMB No. 0704-0188

1. AGENCY USE ONLY *(Leave blank)*	2. REPORT DATE	3. REPORT TYPE AND DATES COVERED
	30 August 2000	Scientific No. 4

4. TITLE AND SUBTITLE
Space Systems Environmental Interaction Studies

5. FUNDING NUMBERS
PE: 63410F
PR 2822 TA GC WU DD

Contract F19628-96-C-0144

6. AUTHOR(S)
M. Alvin Morgan, Alan N. Donkin Jr., John A. Pantazis, Alan C. Huber, Scott J. Moran, David J. Sperry, Robert H Redus

7. PERFORMING ORGANIZATION NAME(S) AND ADDRESS(ES)
AMPTEK, Inc.
6 DeAngelo Drive
Bedford, MA 01730-2204

8. PERFORMING ORGANIZATION REPORT NUMBER

9. SPONSORING/MONITORING AGENCY NAME(S) AND ADDRESS(ES)
Air Force Research Laboratory
29 Randolph Road
Hanscom AFB, MA 01731-3010

Contract Manager: Capt. Wallace R. Turnbull /VSBX

10. SPONSORING/MONITORING AGENCY REPORT NUMBER
AFRL-VS-2001-TR-1660

11. SUPPLEMENTARY NOTES

12a. DISTRIBUTION AVAILABILITY STATEMENT
Approved for public release; Distribution unlimited

12b. DISTRIBUTION CODE

13. ABSTRACT *(Maximum 200 words)*

Pre and post launch support work constitute the most significant activity during the report period. DIDM-2 was launched 15 July 2000 on the CHAMP spacecraft. The inital turn-on and early orbit phase of operations was virtually anomalous-event free, and the instrument continues to return good data. A synopsis of the on-orbit performance to date, is presented in this report. A review of another undertaking, the analysis and design work carried out on behalf of the succeding instrument (DIDM-3), which is to be flown on the Air Force Research Laboratory's Communication/Navigation Outage Forecast (C/NOFS) spacecraft, is also given.

14. SUBJECT TERMS
Digital Ion Drift Meter, DIDM, CHallenging Mini-satellite Program, CHAMP Communications/NAvigation Outage Forcast System, C/NOFS, DIDM-3, Spread-F phenomena, A111F, MOCAD

15. NUMBER OF PAGES
19

16. PRICE CODE

17. SECURITY CLASSIFICATION OF REPORT	18. SECURITY CLASSIFICATION OF THIS PAGE	19. SECURITY CLASSIFICATION OF ABSTRACT	20. LIMITATION OF ABSTRACT
Unclassified	Unclassified	Unclassified	SAR

Table of Contents

List of Figures

1. INTRODUCTION

This contract's objective is to further the understanding of near-earth environmental dynamics, by conducting both *In Situ* experimental studies, as well as, analytical and empirical studies of returned instrument data. The work was to be accomplished through three programs, identified as Task #s 1, 2 and 3. All work on Tasks #s 2 & 3 have ended. A brief review of the scope of Task #1 and a summary of the work performed during the report period follows.

2. TASK #1—DIDM EFFORTS

2.1 Program Definition

The objectives of this task are two-fold. They are: (1) develop the means to reliably measure ion densities in the range of 10^1 cm^{-3} to 10^7 cm^{-3}, by using digital rather than analog techniques, and thereby extend the existing dynamic range for such measurements by at least three orders of magnitude. (2) determine the incident angle of ions into the instrument within 3° in two dimensions, to allow accurate determination of ion drift velocities.

The work performed during the report period falls within Phase 3 of this task, under which a Digital Ion Drift Meter (DIDM-2) instrument was fabricated and tested. The instrument was built for AFRL and delivered to the German research organization GeoForschungsZentrum (GFZ), for inclusion in their earth studies research satellite — the CHAllenging Minisatellite Payload (CHAMP), instrument suite. CHAMP was successfully launched near the end of the report period and DIDM-2 continues to return good data. The instrument will be integral to the global earth magnetic and electric field mapping aspect of the CHAMP mission.

Additional Phase 3 work under this task is the fabrication and test of the successor instrument (DIDM-3), which is to be flown on an AFRL sponsored mission — on the Communication/Navigation Outage Forecast System (C/NOFS) spacecraft, to be launched in the September 2003 timeframe. The mission is an entirely AFRL endeavor, and is intended to characterize and map specific phenomena in the equatorial regions of low earth orbit (altitude to be 400-700km). DIDM-3 will be one of the main environmental diagnostic instruments on-board, and will provide information on ion density, density fluctuations (scintillation), ion drift velocity, as well as collaborative data on the in-situ electric field, which will all serve to greatly enhance the information available to study the so-called *spread-F* phenomena, and ultimately lead to the design of measures to overcome its debilitating impact on the performance of communication, navigation and surveillance systems that rely on signals propagating through this region of the ionosphere.

2.2 Summary of Activities

The activity of greatest significance during the report period was the pre and post launch support for the DIDM-2 instrument on the CHAMP spacecraft. Amptek, Inc. personnel were involved in the spacecraft's system environmental test program, as well as in the diagnosis and resolution of a few anomalous occurrences that arose during the course of the pre-launch system checkout activities. A synopsis of the instrument's on-orbit performance is presented in the following section, 2.3. The other significant effort was the analysis and design work performed on the DIDM-3 instrument. A review of this undertaking appears in Section 2.4.

2.3 DIDM-2 on CHAMP

Following a successful and largely uneventful spacecraft integration with the booster campaign at the Plesetsk Cosmodrome in Russia, CHAMP was launched into polar orbit on June 15th 2000. One week later, Amptek, Inc. personnel traveled with the AFRL/VSBS support team to the German Space Operation Control (GSOC) center in Oberpfaffenhofen outside Munich, for DIDM turn-on. To the very pleasant surprise of all involved, the instrument's response during the turn-on sequence of events, through the initial operations checkout period and indeed its continuing performance to date, has been outstanding. That this came as a bit of a surprise is because some performance anomalies were observed after the instrument was integrated on the spacecraft, during the course of the system integration tests. One such anomaly even occurred during the payload checkout sequence, after spacecraft integration with the launcher at Plesetsk. It transpired however that there was no need to worry. The instrument powered up on queue after launch and has been power cycled multiple times on-orbit thus far, but it continues to perform nominally thus far.

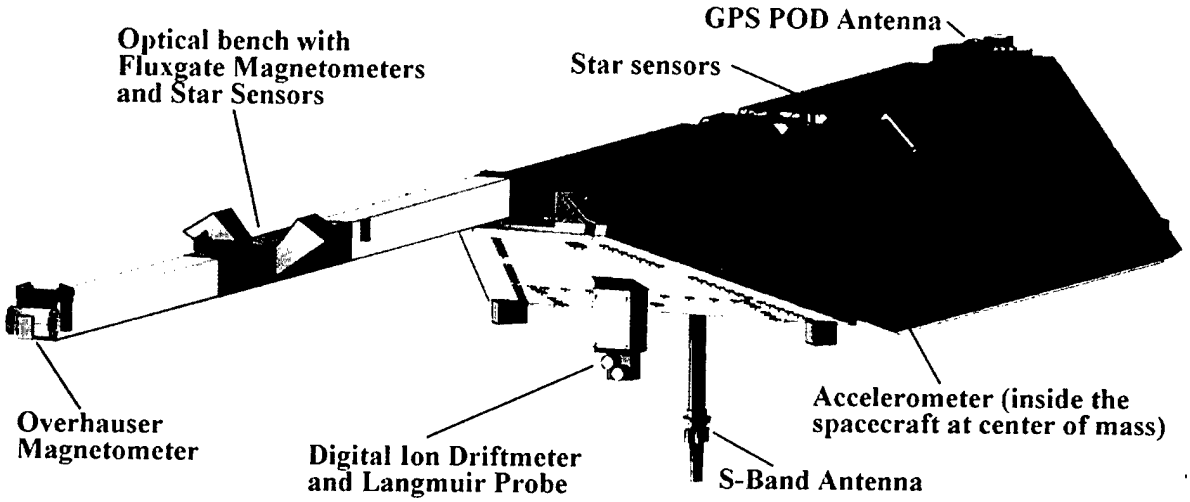

Figure 1: Digital Ion Drift Meter (DIDM-2) with Langmuir Probe on CHAMP spacecraft

The one area in which the instrument's performance is unsatisfactory is in the behavior of one of its two sensors. The sensors were designed and built by the Space Physics group at AFRL and were provided as Government Furnished Equipment to Amptek, Inc. for incorporation onto the otherwise Amptek designed and built instrument (including the key sensing element in the sensors - the position-sensitive wedge and strip anode). The problem with sensor "B" is clearly not with the anode however, which is working as it should. In fact, this sensor's behaviour was known to be different from that of Sensor "A" at instrument delivery, in that a so-called "hot spot" was observed to appear in the Sensor B's response to incident ions, in the calibration chamber. The origin of this spurious response could only be guessed at since there was not enough time to explicitly determine its origin after it first appeared. Furthermore, as it was observed to effectively go away over time under vacuum and was therefore easy to speculate that it was hydroscopic in origin. This implied that a small portion of the surface area within the sensor (presumably either on or in the immediate vicinity of the Micro Channel Plates) developed the capacity to retain moisture (most likely from contamination).

As moisture dissipates (or outgases) in a vacuum, it gives rise to a localized area of enhanced particle density, which in-turn results in a higher response rate of detected events in the sensor. This response falls off with time and it will eventually cease. Such a behavior was observed both in the calibration chamber at AFRL prior to instrument delivery, and in the CHAMP system thermal vacuum testing in Germany. It was also seen in the Sensor "B" response in the early period after instrument turn-on. What has not been observed thus far is a normal response elsewhere in the sensor output. Rather, it appears that the sensor's particle count is down by as much as a factor of ten below what it ought to be. But the number does appear to be gradually increasing. For example, it does appear to be almost twice as high now (at approx. one month after turn-on) than it was in the beginning. Nevertheless, it is clear that the "hot spot" notwithstanding, the sensor's performance has changed greatly from what it was the last time it was stimulated. This is illustrated in Figure 2, which shows in color, the response of the two sensors before and after launch, as seen on the Ground Support Equipment data display. Note the smaller response region for both sensors before launch, due to the small extent of the calibration beam. The "hot spot" response is seen on the outer circle of sensor "B", which is the one on the right.

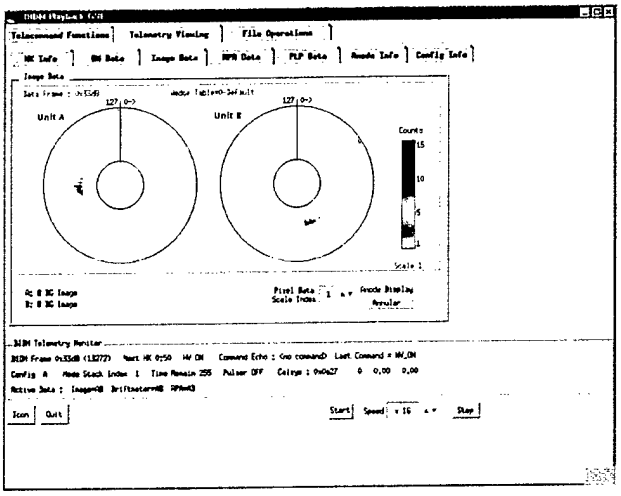

Figure 2(a): Sensor Response before launch

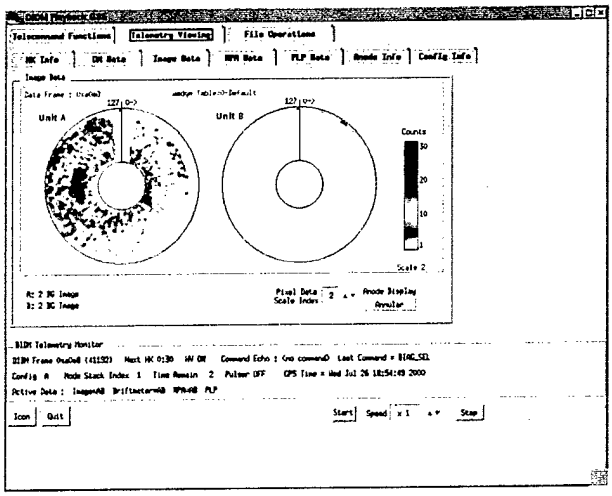

Figure 2(b): Sensor Response after launch

The overall response of sensor "B" is strongly suggestive of a restricted entrance aperture, either by blockage (difficult to realize in a 0.003" dia. hole, as it would seemingly be either fully blocked or not), or by a shift in the various transmission screens which preceed and follow the entrance aperture in the sensor stack assembly, so as to create a Moire pattern that significantly decreases the transmission coefficient of the entire assembly. As this sensor is closest to the relatively large PLP collector, speculation arose also as to whether it is being screened by the floating potential of that surface, but that possibility has largely been ruled out. Speculation is also centered around the fact that there was a premature fairing separation by the launch vehicle, which resulted in unanticipated heating of some elements of the spacecraft. The loss of sun sensors on the vehicle's boom for example, was attributed to this eventuality. The true answer will no doubt emerge in the weeks to come, as the sensor's response to different operating modes is analyzed. The performance of Sensor "B" is of significant interest to the

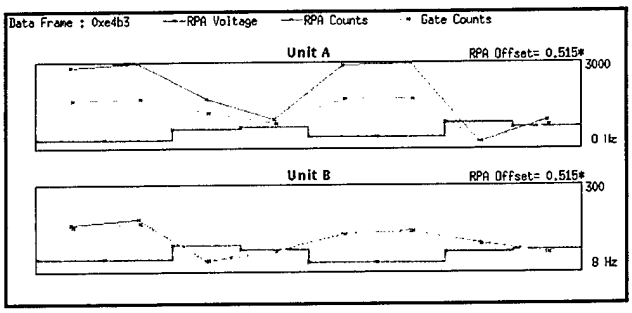

Figure 3(a): RPA Response after launch

DIDM design team at Amptek, because the company is in the process of designing the sensors for the DIDM-3 instrument. It is therefore important that whatever lesson is to be learned about this experience be absorbed and implemented, as to avoid any repetition.

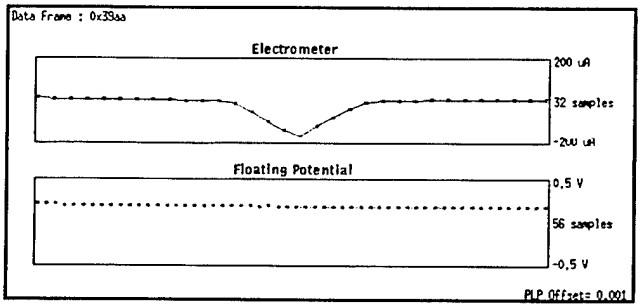

Figure 3(b): PLP Response after launch

Since there is redundancy in having the two sensors in DIDM-2, its scientific mission on CHAMP can, in principle, be fully realized from the data returned by the exemplary performance of Sensor "A" and the PLP. In addition to the Drift Meter (DM) information, an example of which is seen in Figure 2(b), data from the other diagnostic elements within the instrument suite are also being returned. Figure 3(a) shows on-orbit data from the Retarding Potential Analyzer (RPA) and Figure 3(b) shows data from the PLP. The information here is noteworthy, in that a clue to what ails Sensor "B" might be contained in its RPA data plot. It is noted that the Gate and RPA counts are clearly separated for Sensor "A" (as is expected in a regime where the ambient flux is high enough), but they are not separated for Sensor "B". This contradictory bit of information suggests that Sensor "B" is not "seeing" the environment the same way that Sensor "A" does. The RPA plot in Figure 3(a) does however confirm that this diagnostic feature is working properly for both sensors (to the extent that a decrease in counts occurs with an increase in RPA voltage and vice versa). The PLP data confirms a design feature of the spacecraft, in that the floating potential (shown here to be 0.25V) is indeed virtually at the ambient value.

2.4 The DIDM-3 Effort

2.4.1 Summary

The need for another instrument to follow DIDM-2 and a flight opportunity for it, were identified by AFRL early in the report period, and meetings were convened to discuss the requirements for DIDM-3 on the Communication/Navigation Outage Forecast System (C/NOFS) spacecraft. The key enhancement feature identified was the need to increase the image count rate (Drift Meter mode) by at least two orders of magnitude (a factor of 100). This implied that a new anode scheme and associated signal processing electronics would have to be designed. For although considerable time and effort have been put into realizing the position-sensitive wedge and strip anode (which is the key sensing element of the instrument) used on the previous two DIDM instruments, and despite the fact that it has now been flight proven and shown to work exceedingly well, the signal processing circuitry cannot operate at a fast enough rate for the C/NOFS mission. The electronics design is fundamentally inadequate and from a power consumption standpoint, cannot meet the mission objectives.

2.4.2 Segmented Anode Scheme

Ideas on new anode schemes were discussed in depth, and ways to achieve the greatly enhanced throughput were explored. It was immediately clear that one way to achieve the objective was to minimize the necessary amount of anode signal processing, and the idea of utilizing a segmented anode with its output signal going directly into counters, quite quickly rose to the fore. The big driver here though, was the requisite number of pixels needed to realize an adequate image, as both the signal pre-amplifiers and necessary counters could require an overwhelming amount of space on the available printed circuit board real estate inside the instrument housing. This is true not

only by virtue of package size for a large number of devices, but also from the standpoint of routing signals from the anode to the pre-amps and counters. Clearly the greater the number of pixels to be attended to, the greater the circuit layout complexity, as well as, the attendant real estate requirements of the design. An analysis with a minimum-maximum range of pixel numbers was generated to serve as guidance in this effort by the DIDM Principal Investigator at AFRL, Dr. David Cooke, so that some idea of the necessary number of pixels required to do the job was available. With this in hand, a design trade study to asses all the various particulars of parts performance, instrument requirements, design complexibility and manufacturabilty was then carried out.

A full literature search was undertaken of previous work on position sensing anode designs (as reported in the scientific literature), in order to get a full sense of and assess previous approaches to the task, and to possibly arrive at a viable alternative to the wedge and strip design. The first focus for such an alternative was the discrete segment (pixel) design. It satisfied a key requirement, in that it is much easier to fabricate than the wedge and strip – the difficulties encountered in realizing the wedge and strip were legendary in number. The discrete segment design is also inherently fast in operation, as each segment is connected directly to a counter and a minimum amount of signal processing is required. The resolution of a discrete segment design is directly related to the number of segments however, and a large number of segments requires a large number of amplifiers with, as was previously noted, the attendant impact on real estate (size) and power. Amptek's sales catalog for example, lists a very suitable amplifier for the job – the A111F, but there is only one device per package and despite the fact that it is relatively small at 0.655" x 0.375" x 0.115", real estate concerns precluded consideration of its use here, although it is to be used for another purpose in an instrument for which only two units are required.

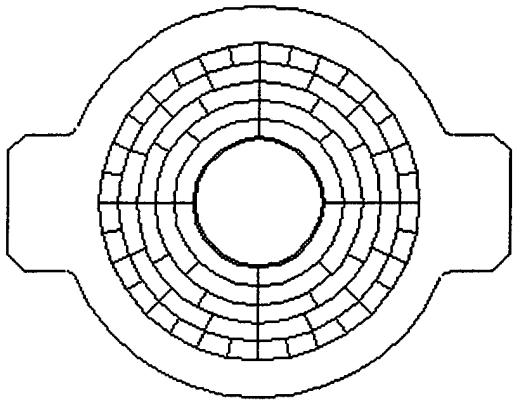

Figure 4: Segmented Anode Design

It was in-fact a European Space Agency designed device, the Monolithic Octal Charge Amplifier/pulse Discriminator (MOCAD), with eight channels in a reasonably sized package, which at first made this design path particularly appealing. It made it practical to realize a design with the minimum number of seventy-two pixels, specified by AFRL for DIDM-3 (see Figure 4 for a proposed anode design layout). However, after carrying out an evaluation of the MOCAD device, it was determined that the arguments against using the device significantly outweighed those in favor. Principal among those against was the MOCAD amplifier performance. It turned out that the eight channels did not have independent threshold control. There is a common threshold adjust per package, but each channel could have an offset that varies by as much as a factor of four from another in the package. This is a major problem, because in order to optimize the design it is desirable not only to have the thresholds as close as possible, but also to have it as low as possible. The largest variation in dynamic range of MCP charge output onto the anode can thus be accommodated. The wide variation in channel thresholds within the MOCAD precluded such an optimization.

Coupled with the considerable printed circuit layout challenge which the design presented (it is not a trivial task to route the signal from each pixel in a fashion such that they do not cross talk and have no appreciable signal path delay as well), and the concerns regarding total power consumption and expense for the required number of amplifiers (at least 25 when units for flight, engineering unit and spares are all factored in), it became apparent that a charge sharing design

which is similar, if not identical to the wedge and strip, would serve us best in this application. For despite the big drawbacks of the wedge and strip (difficult to fabricate and speed of required signal processing), two very big advantages are its inherently high resolution and the fact that it only requires three amplifiers. The challenge remained therefore to maintain the advantages and eliminate the drawbacks in whatever scheme is settled on for the DIDM-3 anode design.

2.4.3 Alternative Anode Schemes

It turns out that many position-sensing anode schemes have been devised. Both the analytic chemistry and astronomy communities appear to have been foremost in developing various ways to make use of the very precise degree of position determination afforded by the technique. An excellent summary of the various anode designs is contained for example, in the book entitled *"State-Selected and State-To-State Ion-Molecule Reaction Dynamics"*, which is a part of an Advances in Chemical Physics Series.[†] In general the various anode techniques can be grouped into two broad classes. These are: (a) discrete segment and (b) charge sharing. Charge sharing anodes can be further divided into at least four classes; i.e.: (i) resistive, (ii) graded density, (iii) capacitive, (iv) wedge and strip, spiral, backgammon etc. There are of course, pros and cons for each technique and arguments for and against the discrete segment design have previously been mentioned. Charge sharing schemes do have the significant advantage of requiring much less than one amplifier per pixel. Indeed the wedge and strip anode requires only three amplifiers, but can be configured to implement an almost limitless number of pixels, with a corresponding degree of measurement resolution. Inherent in this capability therefore, is a very high position resolution capability. Of significant importance in our application is the fact that charge sharing schemes are less dependant on the dynamic range of the output of the micro-channel plates (which provide the anode signal) than the alternatives. They are therefore more conducive to robust detection systems. Among the arguments against charge sharing anodes however are: (a) the fact that the event rate is tied to and may be limited by the signal processing time; (b) depending on the technique employed, there may be significant linearity constraints in using the anode; (c) some anodes of this type are also very difficult to fabricate for large area applications. A brief introduction to a few of the charge-sharing anode techniques follows.

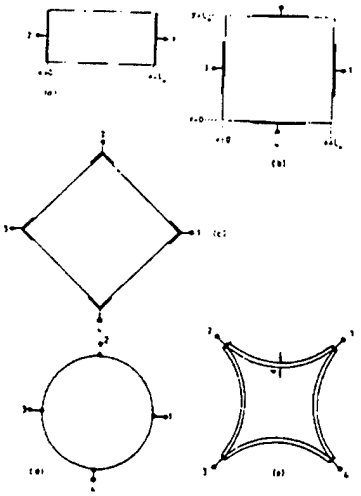

Figure 5(a): Resistive Anode Shapes

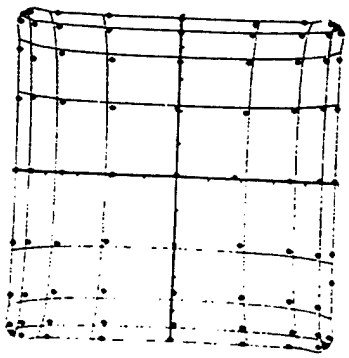

Figure 5(b): Typical Response Map for a Square Anode

[†] See chapter III -*"Position-Sensitive Detection"* in section entitled *"Multicoincidence Detection in Beam Studies of Ion-Molecule Reactions: Technique and Applications to X^- + H_2 Reactions"*, by Jean-Claude Brenot and Marie Durup-Ferguson.

2.4.3.1 Resistive Anode Schemes

Due to their relative simplicity and ease of manufacture, these easily constitute the most commonly used position-sensitive anode type, in part because they have been incorporated into commercially available spectroscopic systems. The basic principle of operation is propagation delay. Incident events closest to the anode terminals are detected earlier in time that events further away, with the time difference being a function of incident location. The biggest problem with this technique is the inherent non-linearity of the output signal, and as a consequence, resistive anodes exist in a myriad of shapes in order to overcome this difficulty. Figure 5(a)[††] illustrates some of the various shapes employed, and a typical response map of a square anode in shown in Figure 5(b). A significant consideration here is that the signal processing for impact position determination can significantly limit the maximum count rate.

2.4.3.2 Graded Density Anode Schemes

This technique relies on coincidencing for position determination. An interlaced pattern of conductive elements is used to detect an incident event, with the response at the output terminals being a unique indication of incident position. A big challenge in designing such a detection system is choosing the proper spacing for the elements to accommodate the anticipated variation in event spot size. Nevertheless, given the appeal of its inherent simplicity, a variety of such schemes have been devised. It can be implemented in as few as two amplifiers, as is shown in Figure 6(a), or more, as is see in Figure 6(b). Signal processing requirements generally ensure that the count rate that can be accommodated is relatively low, and poor position resolution capability has been reported for higher event rates.[††]

Figure 6(a): 2 Amplifier Graded Density Design

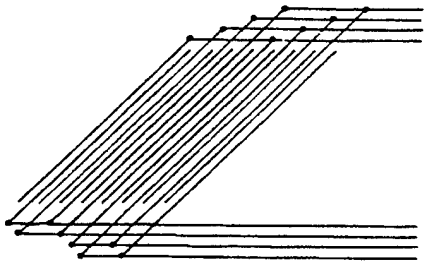

Figure 6(b): 16-Anode, 8 Amplifier Graded Density Design

2.4.3.3 Capacitive Anode Schemes

These employ an alternate coincidencing technique for position determination. The location of an event incident on a grided series of detection elements (identified as numbered strips 0 through 7 in Figure 7, is capacitively coupled to the output terminals in a unique fashion that seeks to minimize the number of amplifiers necessary to indicate which detection element was impacted and where. In the COded Anode CONverter (CODACON) design shown in Figure 7, the topmost amplifier identifies which strip to consider for the incident location by virtue of propagation delay, while the other three amplifiers indicate in binary fashion, where in one of eight locations on each strip the event occurred.

[††] See G. W. Fraser; Nuclear Instruments and Methods in Physics Research 221 (1984) 115-130 *X and γ-Ray Imaging using Microchannel Plates.*

Effectively therefore, with four amplifiers it is possibly to locate the incident location in an 8 x 6 array. Unfortunately, the technique suffers from the same high event rate constraints as the previous coincidencing techniques, and has additional problems as well. They are generally quite difficult to fabricate, and tend to suffer from cross-coupling effects, which especially limit their usefulness at higher count rates. [†††]

2.4.3.4 Other Anode Schemes

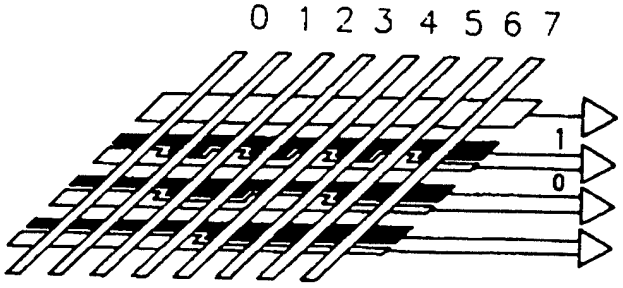

Figure 7: 8-Channel, 4-Amp CODACON Anode Design

In a manner physically similar to the Graded Density anode technique, other schemes employ detector elements of various geometric shapes to generate a unique event response at the anode output, for every possible incident location. A key feature of these techniques is that the output is not inherently discretized. Instead it is analog in nature and an exceedingly high level of resolution can be achieved by essentially binning the output signal into as many levels as desired. Another big advantage of these schemes is that this can be accomplished with very few amplifiers. The prime illustration of the technique is the Wedge and Strip anode, an example of which is shown in Figure 8(a). As it has been implemented in the existing Digital Ion Drift Meter instrument, the output from a geometrical arrangement of three elements (identified as the wedge [W], strip [S] and intermediate area [Z]) is converted by three signal amplifiers only, into a 16 x 128 (2048 element) pixel array (illustrated in Figure 8(b). This translates into azimuth and elevation angle resolution of less than three degrees. Additional pixels and correspondingly higher resolution can be obtained with relative ease, but with a penalty of additional processing capability and power.

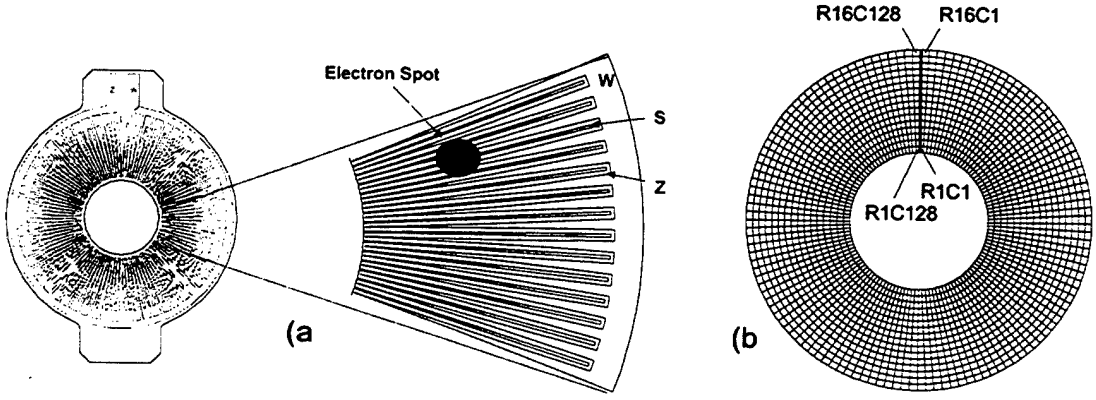

Figure 8: Wedge & Strip Anode detail showing actual structure (a) and equiv pixel array map (b).

There are of course, drawbacks to such techniques as well. The main difficulty is that depending on the intricacies of the pattern and the size of the anode, these devices can be exceedingly difficult (and hence expensive) to fabricate. Indeed, given that the objective is to

[†††] See Richter, Lee J. and Ho, W., . *Multiple Anode Microchannel Array*, Rev. Sci. Instrum. 57 (8) Aug 1986

precisely locate an incident ion (admittedly via the intermediate indicator of a cloud of electrons), the minimum feature sizes of the anode patterns could get to be quite small. In the design shown in Figure 8 for example, the minimum width of a conductive element was five microns (5 μm or 5×10^{-6} m), and the spacing between the three elements was also that small. While such feature sizes are not exactly state-of-the-art these days (which is now on the order of ≈ 0.1 μm), the fact that the anode area must generally be much larger than the typical thumbnail size of most mass produced integrated circuits, ensures that making these devices is a custom, one of a kind production effort. It is also a significant challenge to implement the signal processing necessary to convert the anode output response into event location. This is especially true if there are major power and size constraints to take into account, as is the case in this development effort. Furthermore, depending on the overall complexity of the task, the event count rate of the device could also be seriously compromised.

2.4.3.5 The Backgammon Anode

During the course of researching position sensitive anode types, there was a single standout that satisfied virtually all of the desirability criteria, which are: (a) requires few output amplifiers; (b) has an intrinsically high resolution capability; (c) was of a design that is relatively easy to fabricate. This intriguing hybrid design was referred to as the Backgammon[‡] type, after its obvious

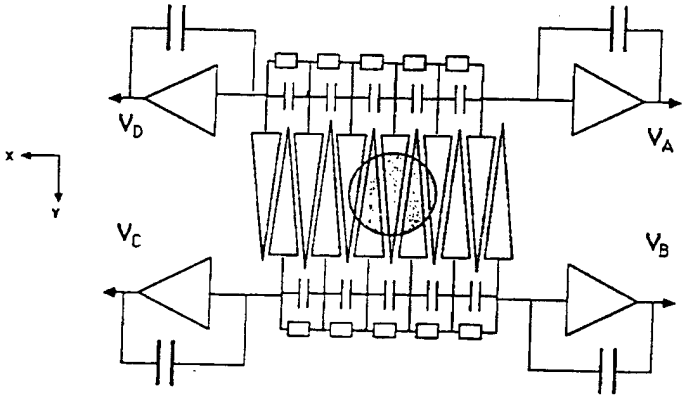

$$X = \frac{Q_C}{Q_A + Q_C} = \frac{Q_D}{Q_B + Q_D} = \frac{Q_C + Q_D}{\Sigma Q_i}$$

$$Y = \frac{Q_A}{Q_A + Q_B} = \frac{Q_C}{Q_C + Q_D} = \frac{Q_A + Q_C}{\Sigma Q_i}$$

Figure 9: Backgammon Anode Scheme and Position Determination Formulation.

similarity to the board game with a similar design. An illustration is shown in Figure 9. It is seen that there are four outputs in the design and hence it requires only four signal amplifiers. The anode pattern itself (i.e. the triangular structures – the solid circle in the middle represents an incident electron cloud) is a very basic one, which implies that the fabrication complexity is minimal. This simplicity also makes it possible for larger feature sizes within the pattern, thus further simplifying the manufacturing task. Yet the position determination measurement technique provides for an almost an infinite degree of measurement resolution in two dimensions. In many ways therefore, the design is an almost ideal solution to the task at hand.

2.4.3.5.1 Backgammon Anode Design

The Backgammon scheme was quickly adopted as the new path along which the anode design was to proceed. The first task was to implement the design in a circular pattern as is required for the sensor assembly and this was quickly done as is illustrated below in Figure 10(a). The detail of how the ends of the separate patterns are terminated is not attended to in the illustration (and hence the very visible gap at the top).

[‡] Roncin, P. Laurent, H and Barat, M., *An electrostatic spectrometer for simultaneous analysis of energy and scattering angle,* J. Phys. E: Sci. Instrum. 19, 37-40 (1986).

But the circular geometry naturally leads to the need to distinguish between 0° and 360° in azimuthal angle, a problem that was previously handled by masking the entire region, so that it was unambiguously clear which side of a *zero-crossing* line incident events occurred. There were however, two problems with this approach. The first is that accommodating the mask adds to the mechanical complexity of the sensor design, and secondly the entire masked region is excluded from the position response portion of the anode. This effectively creates a *blind spot* in the anode response, which, since there must be some size to the mask for it to be effective, cannot be made arbitrarily small. In the DIDM-2 instrument for example, approximately 15° of coverage was excluded from coverage due to the areal extent of the mask, and a requirement of the new design was to minimize that number.

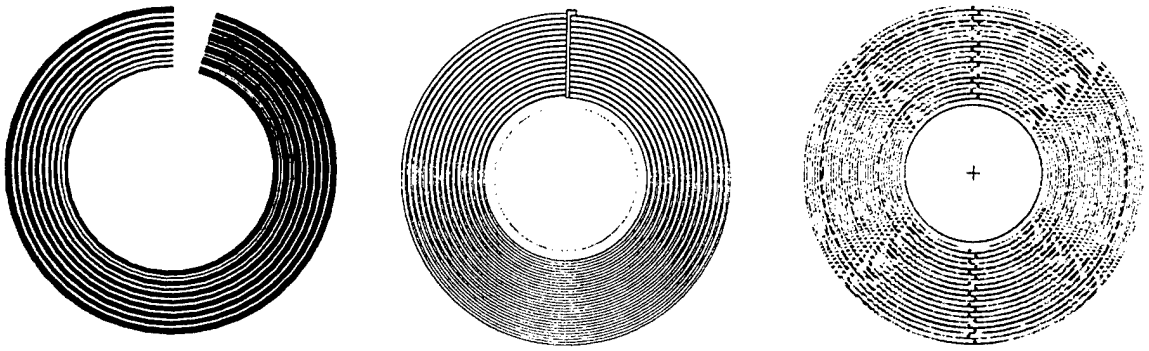

Figure 10: Evolution of Backgammon Anode Design

Indeed the specific requirement was for better than 1% position accuracy over a full 360° extent of incident angle coverage. In an effort to provide the design team with a more quantitative basis for making design trade-off decisions and to get a better handle on design and expected instrument performance, a substantial effort to model, simulate and analyze various design features of the instrument was initiated early in the report period. A new design engineer with substantial experience in using the MATHCAD simulation and analysis tool, was brought on-board to aid in the endeavor. This has proved to be a very useful step. It was conclusively determined for example, that the initial backgammon anode design had an unacceptably high aliasing distortion (error in the determined incident position) in one of two axes, due simply to the layout of the anode pattern. The simulation showed that while this systemic problem could not be easily eliminated, it could be significantly reduced by making a relatively simple change to the pattern. The net result was a calculated change in the loss of accuracy for position determination in the one axis from >2% to <0.25%. Since the design objective is for accuracy within 1%, the change is substantial. The revised change to the anode pattern was immediately adopted.

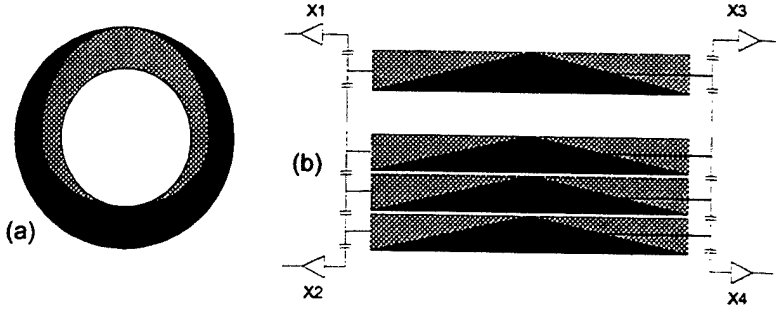

Figure 11: (a) Simulation Model of 2 element Backgammon Anode; (b) element wiring connection detail.

Another area in which the MATHCAD simulation and analysis tool has been put to good use is in the handling of the *zero-crossing* region in the anode design. An extensive study of the performance of various anode design models was carried out,

and it was shown that with a zero-crossing identifier in the design and implemented on the anode surface as shown in Figure 10(b), there will always be an effective azimuthal measurement "dead spot" of approximately 6° minimum. Furthermore, proposals to deal with a zero-crossing region (i.e. linearize the signal response from the area, or simply count incident events) greatly complicate the signal processing electronics design for the instrument. This then led to the development of the continuous element anode pattern as shown in Figure 10(c). A model of the innermost two elements and an illustration of the connections necessary to produce a useful output from the entire pattern, are shown in Figure 11. Note that in actuality these connections will actually occur on the back side of the anode via thru-hole connections from the front or input side.

2.4.3.6 Anode Performance Simulation

At the heart of the modeling effort is a calculation of the total charge deposited on all the collecting elements of the anode pattern (there are thirty six such in the Backgammon design) for a given incident ion event. The element boundaries are defined analytically in polar coordinates.

In the modeling done so far, the separation between them is 1 mil (0.001"), as is the narrowest point of each element. At their widest each element is 15 mils. These dimensions are variable entries in the simulation and are easily changed to reflect other values. The charge cloud is assumed to have a gaussian distribution of charge density (represented by $f(\rho,\phi)$ with ρ being the elevation and ϕ the azimuthal angle respectively), characterized by the standard deviation σ, and the centroid of the charge distribution in radial coordinates, μ_ρ and μ_ϕ. The $(1/(2\pi\sigma^2)$ term normalizes the expression, so that the integral over all coordinates is unity. The charge on each half of the collecting elements is computed numerically by the two double integral expressions shown, which integrate the gaussian charge distribution between the limits set by the element boundaries. From the eighteen collecting elements the charge in the four preamps is computed assuming simple charge division as follows:

$$f(\rho,\phi) := \frac{1}{2\cdot\pi\cdot\sigma^2}\cdot e^{-\frac{\left[(\rho\cdot\cos(\phi)-\mu_\rho\cdot\cos(\mu_\phi))^2+(\rho\cdot\sin(\phi)-\mu_\rho\cdot\sin(\mu_\phi))^2\right]}{2\cdot\sigma^2}}$$

$$QP_i := \int_0^{2\cdot\pi}\int_{\rho LP(\phi,i)}^{\rho UP(\phi,i)} f(\rho,\phi)\cdot\rho\, d\rho\, d\phi$$

$$QM_i := \int_0^{2\cdot\pi}\int_{\rho LM(\phi,i)}^{\rho UM(\phi,i)} f(\rho,\phi)\cdot\rho\, d\rho\, d\phi$$

$$X1_k := \sum_i QP_{i,k}\cdot\frac{i+1}{N} \qquad X3_k := \sum_i QM_{i,k}\cdot\frac{i+1}{N}$$

$$X2_k := \sum_i QP_{i,k}\cdot\frac{N-(i+1)}{N} \qquad X4_k := \sum_i QM_{i,k}\cdot\frac{N-(i+1)}{N}$$

This calculation gives the four preamp outputs for a given event location. To determine the imaging performance over the complete anode, this calculation was carried out at 15,000 points. The coordinates were randomly selected to avoid any possible aliasing effects. The radius and angle were independently selected with a uniform random distribution, from 280 to 510 mils in radius. This leads to somewhat more points per unit area at smaller radii, so the points are not actually distributed uniformly in area. The spot sizes were randomly varied between 10 and 20 mils in radius. The result was a large number of X1, X2, X3, and X4 values and from these Azimuth (ϕ) and Elevation (ρ) are calculated from the following expressions:

$$\phi \approx \frac{(X1+X2)-(X3+X4)}{X1+X2+X3+X4} \qquad \rho \approx \frac{(X1+X3)-(X2+X4)}{X1+X2+X3+X4}$$

which vary from about 0.1 to 0.9 in value. Scale factors to convert these into physical units, degrees of azimuth and elevation, were found by doing a linear regression between the computed "Azimuth" and the actual azimuth, and similarly for elevation, for that region of the anode where a linear response was found. The results are shown in Figure 12. Figure 12(a) shows the measured elevation angle (in units of mils for calculation convenience rather than degrees), versus the actual elevation angle. The equivalent plot for azimuthal angle (in degrees) is seen in Figure 12(b). In both cases the measured values are exceedingly close to the actual values, with some random spreading being evident and small systematic distortions occurring at the ends. It can clearly be seen that over the central portion of the anode, between radii of about 310 to 485 mils, there is no systematic distortion. Outside of the central region where systematic errors are seen, smaller charge clouds have small errors over a larger region of the anode, as one would expect and thus it is only the largest spots, >20 mil, that produce elevation errors below 310 and above 485 mils. This distortion is due to events that are incident close to the edge of the anode pattern and do not fully contribute to the charge collected by the anode elements. Figures 12(c) and 12(d) indicate the error in the calculated elevation and azimuthal angles respectively. If the regions with systematic distortion (wings) are excluded, the calculated elevation angles have a spreading of well under 0.1 mil, which is equivalent to 0.02°. At this level, these residual fluctuations could very well be numerical artifacts. Correspondingly, the azimuthal calculations show a spreading of well under 0.05°.

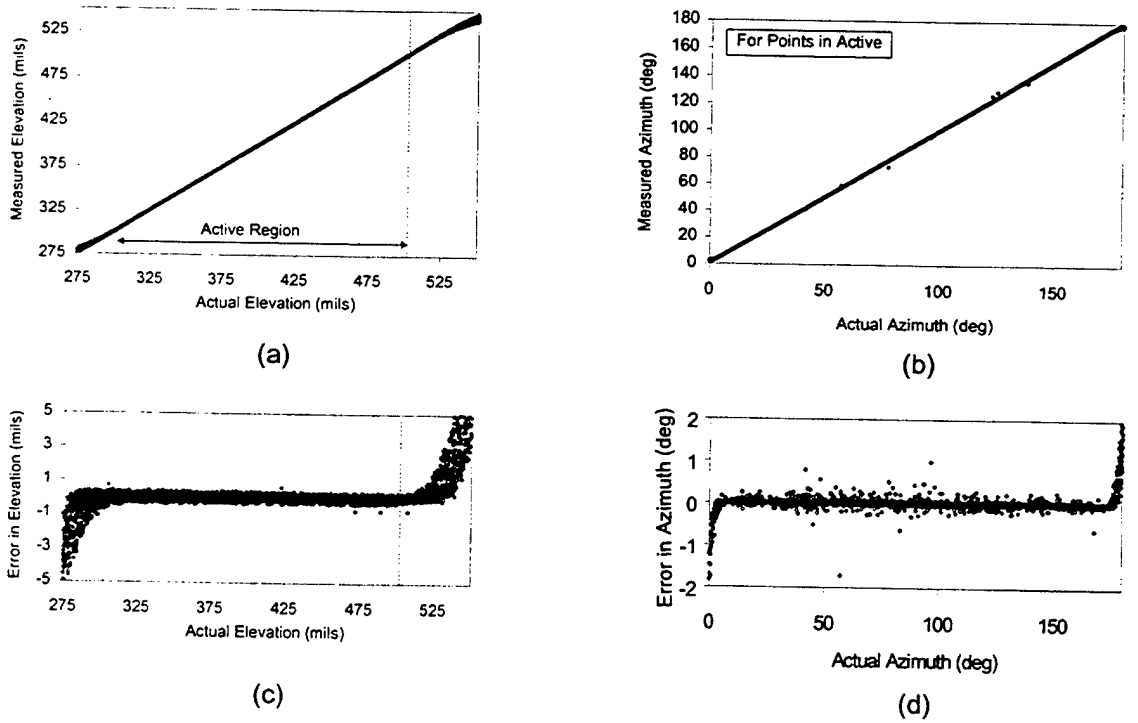

Figure 12: Anode Model Simulation Results

The simulation results also clearly demonstrate the dependance of the anode response on the size of the electron cloud of each incident event. This is especially clear in the aliasing results. Aliasing is the error incurred in reporting the fixed angle (azimuth or elevation) of incident events

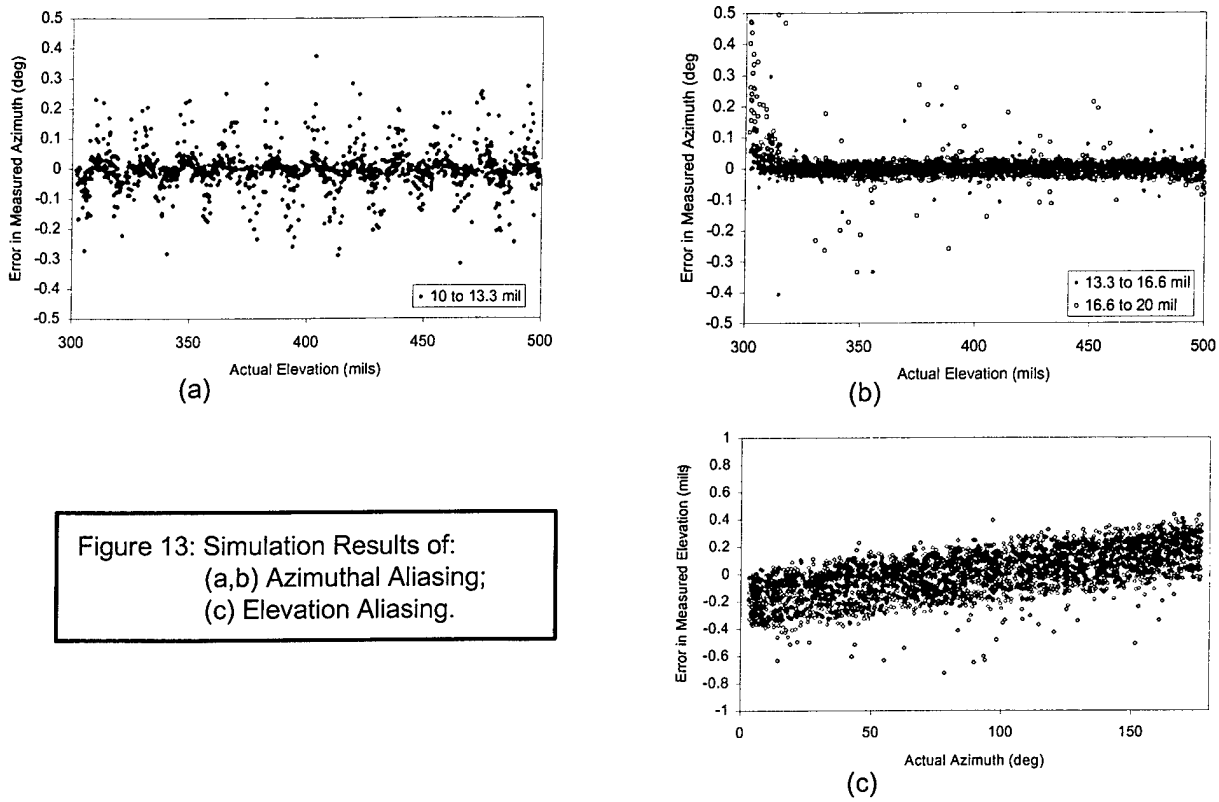

Figure 13: Simulation Results of:
(a,b) Azimuthal Aliasing;
(c) Elevation Aliasing.

when the other angle (elevation or azimuth) varies. It occurs when a significant portion of the event charge falls on a single anode element, and it is readily anticipated for example, if one imagines a series of incident events occurring along a line of constant azimuth but increasing elevation. In such a scenario it can be expected that there would be some systematic non-linearity (usually referred to as aliasing) in the anode response. A clear illustration of this is seen in Figures 13(a) and 13(b) which show the calculated error in azimuthal position when the elevation of the incident event is varied for the anode design shown in Figure 10(c). The aliasing effect appears in the sinusiodal response in the otherwise linear region and as can be seen, the extent of the wiggle is very much a function of event spot size. It is more pronounced the smaller the spot size. In addition, the spatial period is related to the separation between the collecting elements of the anode, between radii of about 310 to 485 mils, about 310 to 485 mils, there is no systematic distortion. It is not so obvious however, that there will be a similar effect for a series of incident events along a line of constant elevation but increasing azimuth (elevation aliasing). But the simulation makes it clear that it does occur as well, although it is was considerably minimized in the final version of the backgammon anode design. The simulation results are illustrated in Figure 13(c), which is a plot of Elevation error versus varying Azimuth location. It is seen that while there is a well defined band for the error, the systematic fluctuation is not as significant as it is only about ± 0.25 mils, which translates to $\pm 0.04°$ given the relationship of acceptance angle to anode coverage space. One significant conclusion from the simulation effort therefore is that although aliasing is inherent in any position sensitive anode design, it can be successfully minimized. Indeed, a key design trade-off which must be made is that of reducing the feature size of the collecting elements and the separation between them (to accommodate increasingly smaller electron clouds and hence minimize the aliasing effect),

and the related complexity of the anode design (which makes it more difficult and hence expensive to fabricate).

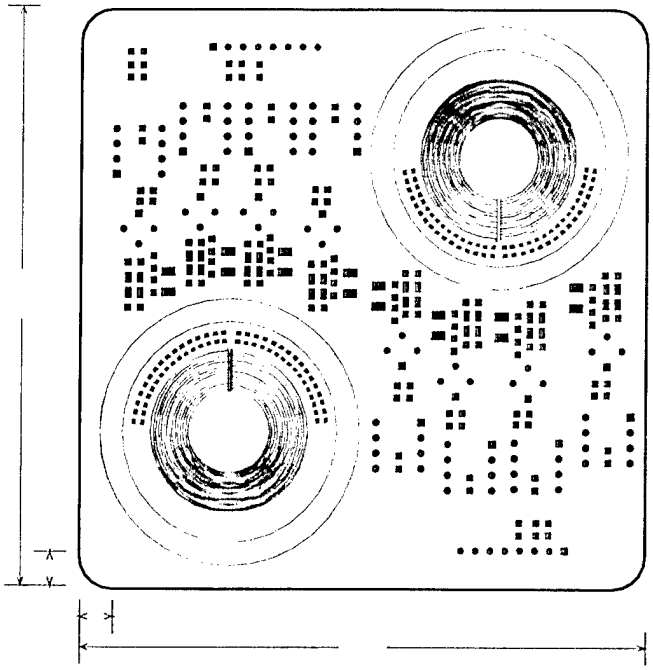

Figure 14: Anode Board Layout Design

2.4.4 New Sensor Design

A great deal of work was carried out on the various elements of the new sensor design for DIDM-3 during the report period. Unlike the case in previous DIDM instruments, for which the sensors were essentially stand-alone elements, the DIDM-3 sensors are integrated into the instrument and the primary sensing element (the backgammon anode) is to be fabricated onto the top-most printed circuit board in the instrument stack. The ability to do this was facilitated by the much larger feature sizes of the collection elements in the new anode design (1 mil minimum feature dimension and 0.5 mil spacing), in comparison to the previous design, which had a minimum feature dimension and spacing of 5 μm (0.2 mil) throughout the anode space. The surface finish necessary to accurately achieve this level of tolerancing cannot be readily achieved on the ceramic material under consideration for use here. Instead, the more suitable (and expensive) quartz material was used, and as it was most expedient to use only as much of the material as was absolutely necessary, having separate standalone sensors was the obvious choice. Figure 14 shows the proposed layout of the two anodes (dense circular patterns) along the diagonal of the ceramic board, amidst the pads for the amplifier components that will process the anode signals.

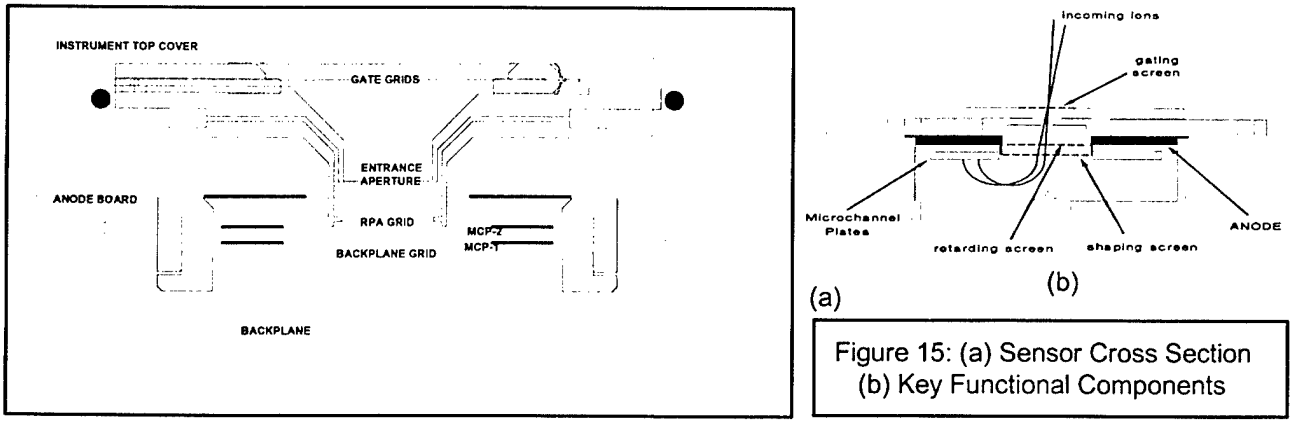

Figure 15: (a) Sensor Cross Section (b) Key Functional Components

The principal sensor related effort however, was on the mechanical design aspects of the sensor assembly itself. A cross-sectional view of the design is shown in Figure 15(a) and a schematic of the essential functional elements is shown in Figure 15(b). From the top, each sensor is comprised of a Gate Grid, which can be raised or lowered in potential to allow ions into the sensor, and an entrance Aperture. Following that, there is a Retarding Potential Analyzer (RPA) grid which can serve as an ion energy discriminator and a Backplane Grid that defines the upper boundary of the optical focusing region within the sensor. The Backplane wall at the bottom in Figure 15(a)

defines the rest of the region. The key detection elements shown are the chevron pair of MicroChannel Plate (MCP) detectors and the position sensitive anode in the Anode Board. An ion entering the assembly is thus focused (in a fashion analagous to the operation of a pin-hole camera) onto the MCP, which in turn produces an electron cloud output that falls onto the backgammon anode. The anode signal is subsequently processed by the electronics within the instrument to determine the incident parameters of the detected particle. As a consequence of the experience gained from working with the previous DIDM sensors, a major driver for this re-design effort was the need to facilitate ease of sensor assembly. The previous sensors were exceedingly difficult to work on and put together. There were numerous and intricate subassembly steps which made the assembly process a lengthy one. While it remains the case that there are many different parts to the new assembly, the process of putting it all together has indeed been greatly simplified. As can be seen from Figure 16, the design is a modular one, with distict halves above and below the sandwiched anode board. Both halves can be individually assembled and then put together with the Anode board to complete the process.

It has to be mentioned that despite the considerable changes, some commonality was necessarily maintained with the previous design. In particular, every effort was made to ensure that the *ion optics* features in the design remain unchanged. That is, the exact dimensions of those components that give rise to the curved portion of the incident trajectory shown in Figure 14(b) were maintained. This includes the Backplane wall dimensions for example, as well as the spacing between the backplane and the incident MCP. Much effort went into simulating trajectory paths for the previous sensor design and given that on-orbit results appear to be bearing out the validity of that functionality, it was critical to ensure that this aspect of the re-design stayed the same. Associated with this concern is the alignment of the aperture to the sharp rise shown in the backplane. This *hill* is a key aspect of the focusing feature of the sensor and its alignment to the center of the aperture is very important. The dowels shown in the Backplane assembly drawing in Figure 15(b) serve to ensure that this alignment is maintained to within 0.001 in (1 mil) when the two halves of the sensor come together.

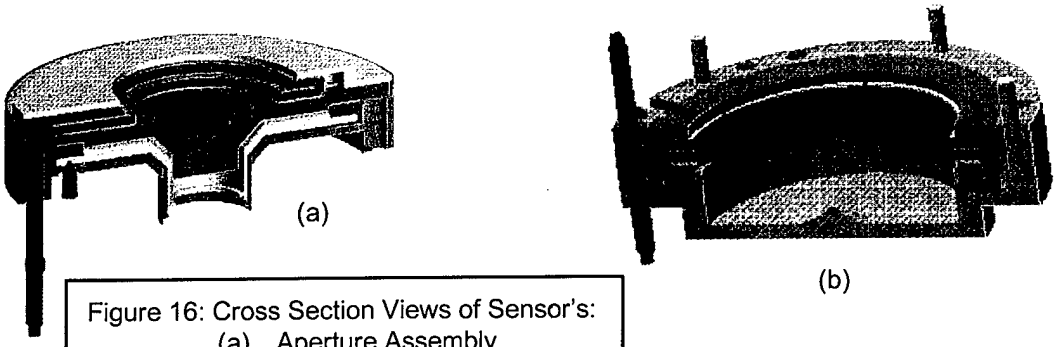

Figure 16: Cross Section Views of Sensor's:
(a) Aperture Assembly
(b) Backplane Assembly

Also settled in the new sensor design is the matter pertaining to perhaps the most important component within the sensor assembly itself. Namely the Micro Channel Plate (MCP) detection element. After much discussion and some negotiation, one amenable domestic manufacturer of MCPs, Burle Electro-Optics of Sturbridge, MA, was identified as being able to provide custom MCPs for the DIDM-3 effort. These devices will be quite different from the company's standard catalog offerings, in that one of the two elements which make-up a functional MCP unit (the so-called "chevron" stack), will be uniquely segmented into two halves with a small (0.020") gap between them. Furthermore, the devices will be of their enhanced performance type and satisfy operating requirements that are near the limit of what is practically realizable.